Journal of Materials Chemistry A

RSC Publishing

PAPER

View Article Online
View Journal | View Issue

Cite this: *J. Mater. Chem. A*, 2013, **1**, 10979

Amyloid-like peptide nanofiber templated titania nanostructures as dye sensitized solar cell anodic materials†

Handan Acar,‡[a] Ruslan Garifullin,‡[a] Levent E. Aygun,[b] Ali K. Okyay[ab] and Mustafa O. Guler*[a]

Received 18th April 2013
Accepted 10th July 2013

DOI: 10.1039/c3ta11542a

www.rsc.org/MaterialsA

One-dimensional titania nanostructures can serve as a support for light absorbing molecules and result in an improvement in the short circuit current (J_{sc}) and open circuit voltage (V_{oc}) as a nanostructured and high-surface-area material in dye-sensitized solar cells. Here, self-assembled amyloid-like peptide nanofibers were exploited as an organic template for the growth of one-dimensional titania nanostructures. Nanostructured titania layers were utilized as anodic materials in dye sensitized solar cells (DSSCs). The photovoltaic performance of the DSSC devices was assessed and an enhancement in the overall cell performance compared to unstructured titania was observed.

1 Introduction

Solar energy is an important source of sustainable energy. Dye sensitized solar cells (DSSCs) are promising and inexpensive alternatives to silicon based solar cells.[1] Although there are many semiconductor materials available for constructing DSSCs, titania (TiO_2) is the most widely used owing to several advantages such as abundance, biocompatibility, eco-friendliness and inexpensiveness.[2] DSSCs have several components for light harvesting, electron transport, and hole transport. The optimization of each component affects the overall performance of the cell.[3] Since electrons and holes are transported in different media, separate optimization at each interface can be studied to enhance the yield of DSSCs. There are several parameters used to enhance the efficiency of DSSCs including the TiO_2 component such as obtaining a pure anatase phase, greater surface area for better dye adsorption, hole conduction, higher pore volume and diameter, and well-connected network of individual nanostructures.[4,5] On the other hand, the application of TiO_2 nanoparticles in DSSCs limits the power conversion efficiency of DSSCs by electron trapping in the nanostructured film. The time scale for injection and transport of the electron by TiO_2 is comparable with the time scale of the recombination by the electrolyte.[6] The competition between these time scales determines the photon-to-current conversion efficiency of the DSSC. One of the major problems of DSSCs is this loss of electrons at the TiO_2–electrolyte interface.[7]

The transport of charge carries through the one-dimensional morphology of a TiO_2 electrode is more facile because of its inherent nature to produce lower diffusion resistance.[8] One-dimensional nanostructures including nanowires[9] and nanorods[10] are able to transport electrons before the recombination process takes place.[11] Highly ordered architectures offer longer electron diffusion paths and shorter electron transport time constants than randomly oriented titania nanoparticle films.[12] In fact, cylindrical (nanowire) and tubular (nanotube) architectures act as a "box" that delimits the medium through which the electron travels. If the diameter of the "box" is smaller than the mean free path of the electron, enhancement in electron mobility could be expected.[13]

Proteins and peptides can assist synthesis of nanostructured inorganic materials in an eco-friendly strategy *via* a biomineralization process. Nature inspired synthetic peptide nanofiber networks have wide applications including in bioactive tissue scaffolds,[14,15] carrier agents,[16,17] and template-directed synthesis of inorganic materials.[18] Self-assembled amyloid-like peptides (ALPs) can be successfully used to obtain one-dimensional inorganic nanostructures,[19,20] which may find applications in electronics[21] and sensors.[22] The synthesis of TiO_2 hybrid nanowires using amyloid protein fibrils as templates, and their application in hetero-junction hybrid solar cells were previously reported.[23] The peptide assemblies can be effectively used as soft templates for the synthesis of inorganic and organic–inorganic hybrid nanostructures.[24] Previously, we demonstrated titania and silica mineralization on self-assembled ALP templates.[19]

Here, we demonstrate peptide nanofiber templated synthesis of TiO_2 nanostructures. A bottom-up approach,

[a]*Institute of Materials Science and Nanotechnology, National Nanotechnology Research Center (UNAM), Bilkent University, Ankara, 06800, Turkey. E-mail: moguler@unam.bilkent.edu.tr; Fax: +90 312 266 4365; Tel: +90 312 290 3552*

[b]*Department of Electrical and Electronics Engineering, Bilkent University, Ankara, 06800, Turkey*

† Electronic supplementary information (ESI) available. See DOI: 10.1039/c3ta11542a

‡ These authors contributed equally.

realized through a mineralization process of self-assembled organic templates, leads to a high-surface-area hybrid titania nanofiber network. Calcination of the hybrid material network on the surface of fluorine doped tin oxide (FTO) coated glass yields a functional electrode with a nanostructured anatase titania layer. Staining of the obtained titania layer with N719 photosensitizer dye provides it with photoactivity. The photoactivity and overall performance of functional devices based on our engineered materials were assessed for dye sensitized solar cell applications. One-dimensional TiO_2 nanostructures synthesized with self-assembled peptide templates exhibited high surface area with abundant mesopores, which is convenient for high dye loading, and also exhibited improved open circuit voltages (V_{oc}); as a result, enhanced photovoltaic performance was observed compared to peptide nanofiber template-free TiO_2 particles.

2 Experimental

2.1 Materials

The peptides were designed and synthesized as reported previously.[7] Fmoc and Boc protected amino acids, MBHA Rink Amide resin, and HBTU were purchased from NovaBiochem and ABCR. The other chemicals were purchased from Fisher, Merck, Alfa Aesar or Aldrich and used as received. The 3 mm thick fluorine doped tin oxide (FTO) coated glass (sheet resistivity of 8 Ω sq^{-1}), photosensitizer dye Ruthenizer 535-bis TBA (N719), Iodolyte AN 50 electrolyte and Meltonix 1170-60 thermoplastic were purchased from Solaronix.

2.2 Characterization

Transmission electron microscopy. Imaging of the peptides was carried out by bright-field TEM (FEI, model Tecnai G2 F30) operated at 100 kV. Uranyl acetate solution in ethanol (2 wt%) was used for peptide nanofiber staining.

X-ray diffractometry. TiO_2 powder X-ray diffraction (XRD) patterns were obtained by using Cu-Kα radiation on a Panalytical XPert-PRO (reflective mode) equipped with an X'Celerator Scientific RTMS detector.

Porosity measurements. The surface areas of the TiO_2 powder samples were determined by BET analysis carried out in an Autosorb-iQ Station.

Photovoltaic measurements. Photovoltaic current–voltage (*J–V*) measurements of the solar cells were taken from the active area of 0.25 cm^2 (0.5 cm $\times$ 0.5 cm). Cells were scanned between (-1, 1 V) and (-100 and 100 mA). A Newport full spectrum solar simulator with air mass (AM) 1.5 filter from Oriel was used as a light source in the *J–V* measurements. The simulator was operated at the following parameters: AM 1.5 G, 100 mW cm^{-2} and 25 °C.

Inductively coupled plasma-mass spectrometry (ICP-MS) analysis. A ThermoFisher PlasmaLab ICP-MS was used. All of the DSSCs were disassembled after photovoltaic measurements. The TiO_2 on the FTO was digested in hydrofluoric acid (HF). 50 μL of 48% HF was dropped onto the TiO_2 film and incubated for 10 min in polyethylene dishes. Solutions were diluted for the ICP-MS analysis.

Dye adsorption measurements. The amount of the dye adsorbed on the electrodes was measured by a Cary 100 UV spectrophotometer. For desorption of dye from the TiO_2 surface, 1 : 1 ethanol–0.1 M NaOH solution was prepared.[25–27] Each cell was immersed in 3 mL of 1 : 1 ethanol–0.1 M NaOH solution for 1 h for desorption of the dye. Six different N719 dye samples were prepared in this solution as 0.01, 0.05, 0.1, 0.5, 1 and 5 μM in 3 mL. The absorption spectrum of 5 μM N719 dye in this solution was observed at 515 nm (Fig. S12†). The calibration curve of the standards was calculated by taking the intensity of absorption at 515 nm and $R^2 = 0.993$ (Fig. S13†).

Diffuse reflectance measurements. Diffuse reflectance spectra of the TiO_2 materials were recorded by a Cary 5000 UV-Vis-NIR spectrophotometer with an internal diffuse reflectance attachment. A powder cell was used for the analysis.

2.3 Nanostructured TiO_2 paste preparation

1 wt% peptide gels were prepared (5 mg of peptide in 500 μL of ethanol) and aged overnight. Then, the gels were diluted by the addition of 500 μL of ethanol and 5 molar equivalents of titanium(IV) isopropoxide [$Ti(O\text{-}iPro)_4$] (Alfa-Aesar) was added as a titanium precursor to the self-assembled peptide nanofibers in ethanol. The samples were incubated for 24 h at room temperature in closed vials. The mineralized gels were washed with methanol and centrifuged several times. The titania nanostructures were dispersed in 500 μL of ethanol and to this mixture 250 μL of α-terpineol (Alfa Aesar) and 500 μL of ethyl cellulose solution (Alfa Aesar, 10% in ethanol) were added. The final mixture was used as a nanostructured TiO_2 paste.

2.4 Solar cell assembly

TiO_2 pastes were applied onto the surface by drop casting due to lack of adequate viscosity. All of the TiO_2 applied onto the FTO glasses was calcined at 450 °C for 2 h. The calcined FTO glasses were soaked in 0.03 mM N719 dye for 24 h. 25 nm Pt coated glass surface was used as the counter-electrode. Iodolyte AN 50 was used as an electrolyte and was injected between the electrodes of the solar cells.

3 Results and discussion

Amyloid-like peptides (ALPs) are able to self-assemble into one-dimensional nanofibrillar structures through supramolecular interactions between individual peptide molecules. Here, two *de novo* designed peptides (Fig. 1 and S1–S4†) with high binding affinity to metal ions were used in the synthesis of nanostructured TiO_2. The nanostructured TiO_2 was obtained through a bottom-up approach, where self-assembled peptide nanofibers (Fig. 1b and d) were used as a template. Amine groups in the lysine residues in peptide **1** (Fig. 1a) and carboxylate groups in glutamate residues in peptide **2** (Fig. 1b) act as nucleation and successive growth centers for TiO_2. Owing to the side chains of the lysine residues, peptide **1** is several atoms longer than peptide **2** (Fig. 1a and b) and the self-assembled

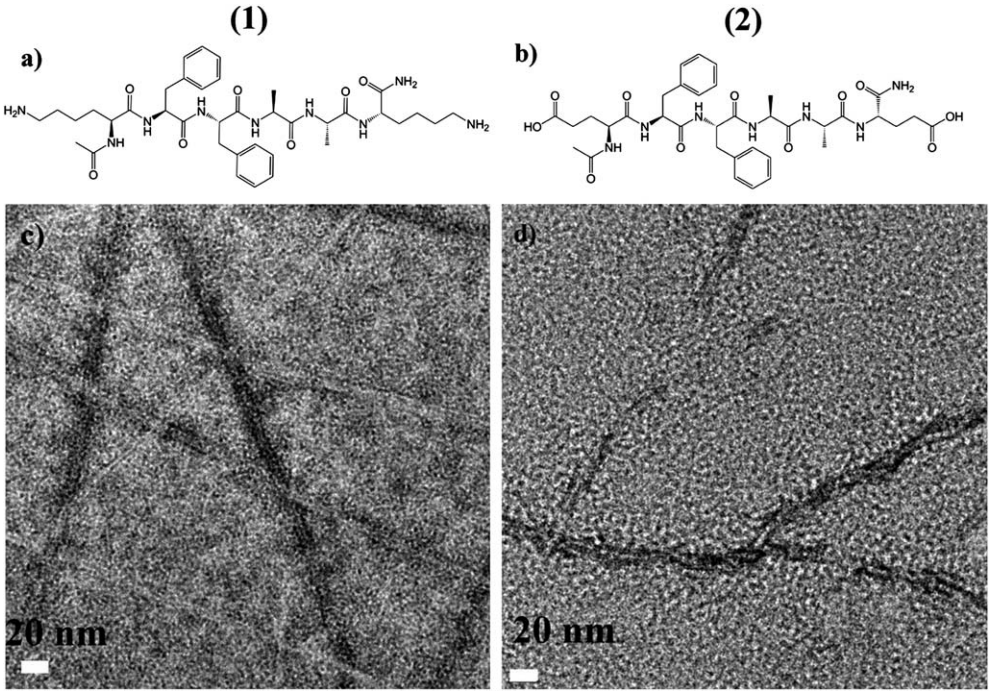

Fig. 1 Amyloid-like peptides. (a) Ac-KFFAAK-Am (peptide **1**), (b) Ac-EFFAAE-Am (peptide **2**), (c) TEM image of the peptide **1** nanofibers, (d) TEM image of the peptide **2** nanofibers.

peptide nanofibers formed by peptide **1** are slightly thicker than the peptide **2** nanofibers (Fig. 1c and d). The average diameters of peptide **1** and peptide **2** nanofibers were found to be 11.4 ± 0.42 and 9.1 ± 0.61 nm, respectively. The difference in nanofiber thickness is dictated by the self-assembly mechanism; while hydrophobic amino acids in the structure of the peptides escape from the polar solvent and bury themselves in the core of the nanofibers, hydrophilic residues, on the contrary, expose them on the nanofiber surface. Solvophobic escape and consequent nanofiber formation is enhanced by π–π stacking of diphenylalanine motifs. Peptide self-assembly and nanofiber surface mineralization both take place in solution, thus making this approach appealing for bulk production procedures. To compare the template-effect of peptide nanofibers and their effect on peptide templated TiO_2 morphology, TiO_2 particles were also synthesized without peptide nanostructures under the same conditions (Fig. S5†).

Exploiting soft nanofibrillar templates in nanofabrication processes enables the synthesis of high-aspect-ratio materials with high surface areas.[18] Here, we obtained a highly porous network of one-dimensional TiO_2 nanostructures by using peptide nanofiber templates (Fig. 2). Due to the shape of the template-directed (110) TiO_2 growth, fast and directional charge transfer to the conductive transparent oxide layer (anode) should be possible. This charge transfer enhancement should substantially decrease the conduction losses, due to recombination processes in the electrode. Moreover, nanostructured titania with a high surface area provides increased interaction between TiO_2 and the dye in DSSC devices. To understand the effect of nanostructured TiO_2 on DSSC photovoltaic performance, three sets of solar cells were built from three different TiO_2 materials (peptide **1** templated TiO_2, peptide **2** templated TiO_2 and template-free synthesized TiO_2). Peptide **1** leads to nanotubular TiO_2 structures, while peptide **2** favors TiO_2 nanowire architecture (Fig. 2a and b). As mentioned above, the lysine residues have longer side chains compared to the glutamate residues. This small difference affects the final diameter

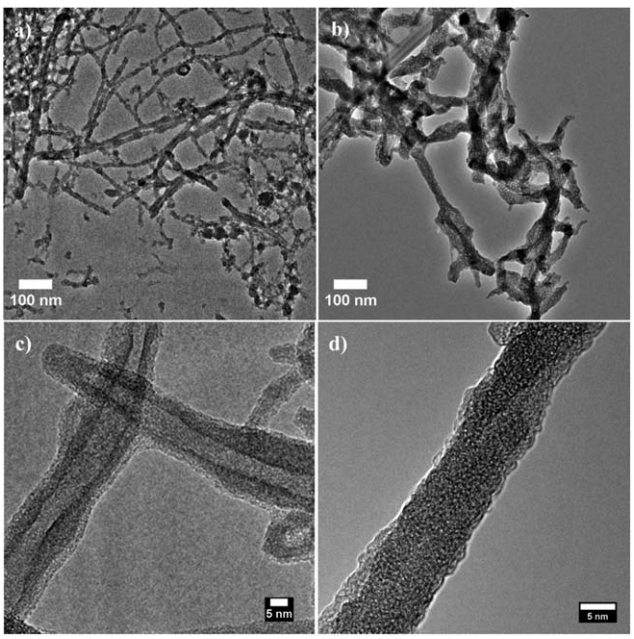

Fig. 2 One-dimensional TiO_2 nanostructures after calcination. TEM images of peptide **1** templated TiO_2 (a) nanotube network and (c) nanotubes; TEM images of peptide **2** templated TiO_2 (b) nanowire network and (d) nanowires.

of the nanofibers. Thicker peptide **1** nanofibers prevent complete sintering of the material into nanowires during the calcination process, therefore nanotubes are observed. The thickness of the self-assembled peptide nanofibers affects the resultant architecture of one-dimensional TiO_2 nanostructures (Fig. 2). It is crucial to obtain one-dimensional TiO_2 in its anatase phase: a semiconductor phase used for DSSC construction. The mineralized titania nanostructures were annealed at 450 °C to produce anatase morphology. The XRD pattern of the anatase phase obtained during the sintering and annealing process is shown in Fig. S7 and S8.† The organic peptide template was removed during the calcination stage. It was previously demonstrated that the thermal decomposition of peptide is completed at 350 °C.[19] Thus, 450 °C is sufficient for both thermal combustion of the organic peptide template and phase transformation of titania.

The calcination process takes place directly on the FTO glass, which minimizes the solar cell assembly steps. Stained with sensitizer (N719), peptide-templated materials were probed in the dye sensitized solar cell experiments. In fully functional solar cell devices, nanostructured titania was sandwiched between two electrodes with the addition of liquid iodine/iodide electrolyte. The amount of TiO_2 on the FTO surface is an important parameter, which affects the overall efficiency of the DSSC. Accurate measurement of the TiO_2 amount was achieved by inductively coupled plasma-mass spectrometry (ICP-MS). The amount of template-free synthesized TiO_2 was found to be about two times greater than the amount of TiO_2 nanowires and nanotubes synthesized by the peptide nanofiber templates. This could be due to the three-dimensional structure of the bulk TiO_2 nanowires and nanotubes (Fig. S6†), which inhibit the sintering and aggregation of titania during the calcination process. On the other hand, since template-free titania particles have no particular shape and size, they re-assemble on the surface during the calcination to form denser aggregates (Fig. S5†). Thus, after the calcination, the amount of adhered TiO_2 on the surface was higher for template-free synthesized nanoparticles.

The specific surface areas of the TiO_2 nanostructures were analyzed by using a nitrogen gas adsorption method, which relies on Brunauer–Emmett–Teller theory (BET).[28] The measurements showed that the surface area of the peptide **1** templated nanotube network was more than five times and the area of the peptide **2** templated nanowire network was more than three times greater than that of template-free synthesized TiO_2 particles (Fig. S9–S11†). The pore size of the TiO_2 in the DSSC should be large enough to allow easy diffusion of electrolyte, while avoiding the recombination of redox species in the electrolyte.[1] Therefore, one-dimensional nanostructures offer the best morphology. Since N719 dye molecules are not likely to aggregate, it could be assumed that the dye should be adsorbed as monolayer;[29,30] therefore, increasing the surface area causes an increase in the amount of adsorbed dye and as a result, enhances the efficiency of the solar cell.[31] The amount of adsorbed dye is expected to be greater for nanotubes and nanowires compared to template-free synthesized TiO_2. Indeed, the average amount of adsorbed dye was found to be three times greater for nanotubes and one and a half times greater for nanowires compared to template-free particles, which does not contradict the surface area measurements (Table 1). Nevertheless, the increase in the dye loading observed for the template synthesized materials is smaller than the increase in the surface area. This incomplete dye loading can be rationalized by imperfect diffusion of the dye into porous structures.

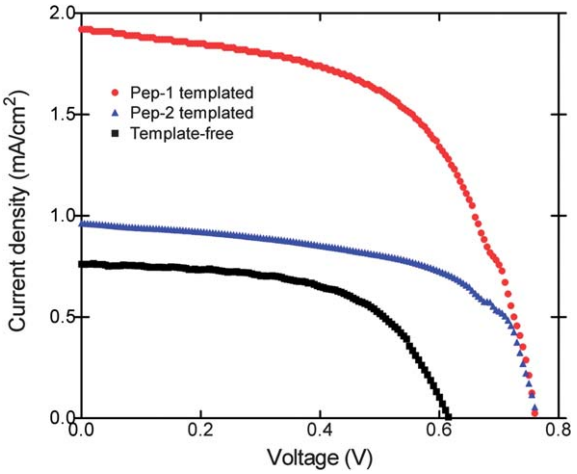

Fig. 3 Representative *J–V* spectra of devices based on peptide **1** (Pep-1), peptide **2** (Pep-2) templated and template-free TiO_2 materials.

The photoconversion efficiencies of the DSSCs were analyzed by a solar simulator set-up. The *J–V* characteristics of the photovoltaic devices are shown in Fig. 3. The devices with nanostructured materials exhibited significantly better photovoltaic performance. The cells produced on peptide **1** templated TiO_2 nanotube electrodes revealed a significant enhancement in the short circuit current compared to peptide **2** templated TiO_2 nanowire electrodes and template-free TiO_2 electrodes. This is attributed to a dramatic increase in the surface area of the electrode. Although the fill factor values were comparable, the open circuit voltage values for the templated materials were around 760 mV, while the template-free synthesized material did not exceed 620 mV (Table 1). The observed V_{oc} enhancement is attributed to bandgap widening caused by the physical

Table 1 Properties of representative DSSCs

TiO_2	J_{sc} (mA cm^{-2})	V_{oc} (mV)	Fill factor	Efficiency (%)	Surface area (m^2 g^{-1})	Adsorbed dye (mmol g^{-1})
Peptide **1**-templated	1.92	760	0.57	0.83	150.63	1.99
Peptide **2**-templated	0.96	765	0.59	0.44	102.94	0.97
Template-free	0.76	620	0.57	0.27	27.01	0.65

confinement of electrons in nanostructured materials. Diffuse reflectance spectra indicate blue-shifted bandgap edges for templated materials (Fig. S14†). This clearly demonstrates the important role of the peptide-templated materials in enhancing the overall efficiency of the device performance.

As discussed above, the efficiency of the DSSC directly depends on the amount of electrodic TiO_2 and the amount of dye adsorbed on the electrode. Thus, the measurement of all of the parameters is crucial for comparing the efficiencies of DSSCs constructed from different TiO_2 structures. Due to the nanostructure properties, TiO_2 nanotubes are capable of adsorbing more dye on their surface. Therefore, the efficiency results were normalized to the amounts of TiO_2 and adsorbed dye (Table S1†). When taking all of the parameters into account, the efficiency of the TiO_2 nanotube network prepared by the peptide **1** template was significantly higher than that of the peptide **2** templated TiO_2 nanowire network (Fig. 3 and Table 1). Also, the efficiency of the DSSC prepared from peptide **2** templated TiO_2 was higher than that of the template-free TiO_2 particles. It should also be noted that the obtained absolute device efficiencies are low and are primarily for comparative purposes. Low efficiencies are the result of poor adherence of titania materials to the FTO surface; only thin layers of anodic titania could be achieved.

4 Conclusions

A green synthesis method of one-dimensional TiO_2 nanostructures for dye sensitized solar cells by using peptide nanofiber templates can offer an attractive and promising method in the growing field of sustainable energy. The differences between the efficiencies of DSSCs prepared using nanotubes, nanowires and template-free nanoparticles were compared and discussed. Using peptide self-assembly and mineralization under ambient conditions enabled the convenient synthesis of titania nanostructures. Self-assembled peptide nanofibers offer unique templating possibilities, which allows the synthesis of nanostructured materials with high surface areas. The mineralization of titania around the peptide nanofibers also occurs by deposition of inorganic ions. Networks of these one-dimensional titania nanostructures possess intriguing features, such as greater surface areas and improved open circuit voltages, which result in enhanced photoactivity. Dye sensitized solar cell experiments have demonstrated the superiority of nanostructured materials and emphasized the importance of a bottom-up approach realized *via* self-assembled soft templates.

Acknowledgements

We would like to thank M. Guler for help in TEM imaging, and Dr M. F. Genisel and S. Kolemen for fruitful discussions. This work was supported by the Scientific and Technological Research Council of Turkey (TUBITAK), grant number 109T603, FP7 Marie Curie IRG and COMSTECH-TWAS grants. M. O. G. and A. K. O. acknowledge a Marie Curie International Reintegration Grant (IRG). R. G. is supported by a TUBITAK-BIDEB PhD fellowship. M. O. G. acknowledges support from the Turkish Academy of Sciences Distinguished Young Scientist Award (TUBA-GEBIP).

Notes and references

1 B. O'Regan and M. Grätzel, *Nature*, 1991, **353**, 737–740.
2 X. Chen and S. S. Mao, *Chem. Rev.*, 2007, **107**, 2891–2959.
3 B. E. Hardin, H. J. Snaith and M. D. McGehee, *Nat. Photonics*, 2012, **6**, 162–169.
4 C. Karthikeyan, M. Thelakkat and M. Willert-Porada, *Thin Solid Films*, 2006, **511**, 187–194.
5 Y. J. Kim, M. H. Lee, H. J. Kim, G. Lim, Y. S. Choi, N.-G. Park, K. Kim and W. I. Lee, *Adv. Mater.*, 2009, **21**, 3668–3673.
6 G. Schlichthörl, S. Huang, J. Sprague and A. Frank, *J. Phys. Chem. B*, 1997, **101**, 8141–8155.
7 H.-J. Son, X. Wang, C. Prasittichai, N. C. Jeong, T. Aaltonen, R. G. Gordon and J. T. Hupp, *J. Am. Chem. Soc.*, 2012, **134**, 9537–9540.
8 M. Grätzel, *Acc. Chem. Res.*, 2009, **42**, 1788–1798.
9 X. Feng, K. Shankar, M. Paulose and C. A. Grimes, *Angew. Chem.*, 2009, **121**, 8239–8242.
10 B. Liu and E. S. Aydil, *J. Am. Chem. Soc.*, 2009, **131**, 3985–3990.
11 K. Zhu, N. R. Neale, A. Miedaner and A. J. Frank, *Nano Lett.*, 2007, **7**, 69–74.
12 O. K. Varghese, M. Paulose and C. A. Grimes, *Nat. Nanotechnol.*, 2009, **4**, 592–597.
13 C. M. Lieber, *Solid State Commun.*, 1998, **107**, 607–616.
14 H. Ceylan, S. Kocabey, A. B. Tekinay and M. O. Guler, *Soft Matter*, 2012, **8**, 3929–3937.
15 H. Ceylan, A. B. Tekinay and M. O. Guler, *Biomaterials*, 2011, **32**, 8797–8805.
16 S. Bulut, T. S. Erkal, S. Toksoz, A. B. Tekinay, T. Tekinay and M. O. Guler, *Biomacromolecules*, 2011, **12**, 3007–3014.
17 R. Garifullin, T. S. Erkal, S. Tekin, B. Ortac, A. G. Gurek, V. Ahsen, H. G. Yaglioglu, A. Elmali and M. O. Guler, *J. Mater. Chem.*, 2012, **22**, 2553–2559.
18 M. A. Khalily, O. Ustahuseyin, R. Garifullin, R. Genc and M. O. Guler, *Chem. Commun.*, 2012, **48**, 11358–11360.
19 H. Acar, R. Garifullin and M. O. Guler, *Langmuir*, 2011, **27**, 1079–1084.
20 P. Tamamis, L. Adler-Abramovich, M. Reches, K. Marshall, P. Sikorski, L. Serpell, E. Gazit and G. Archontis, *Biophys. J.*, 2009, **96**, 5020–5029.
21 H. Acar, R. Genc, M. Urel, T. S. Erkal, A. Dana and M. O. Guler, *Langmuir*, 2012, **28**, 16347–16354.
22 A. Yildirim, H. Acar, T. S. Erkal, M. Bayindir and M. O. Guler, *ACS Appl. Mater. Interfaces*, 2011, **3**, 4159–4164.
23 S. Bolisetty, J. Adamcik, J. Heier and R. Mezzenga, *Adv. Funct. Mater.*, 2012, **22**, 3424–3428.
24 K. Rurack and R. Martínez-Máñez, *The Supramolecular Chemistry of Organic–Inorganic Hybrid Materials*, Wiley, 2010.
25 Z.-S. Wang, H. Kawauchi, T. Kashima and H. Arakawa, *Coord. Chem. Rev.*, 2004, **248**, 1381–1389.
26 M. Hočevar, M. Berginc, M. Topič and U. O. Krašovec, *J. Sol-Gel Sci. Technol.*, 2010, **53**, 647–654.

27 L. González-García, I. González-Valls, M. Lira-Cantu, A. Barranco and A. R. González-Elipe, *Energy Environ. Sci.*, 2011, **4**, 3426–3435.
28 P. Westermark, U. Engström, K. H. Johnson, G. T. Westermark and C. Betsholtz, *Proc. Natl. Acad. Sci. U. S. A.*, 1990, **87**, 5036–5040.
29 R. Katoh, K. Yaguchi and A. Furube, *Chem. Phys. Lett.*, 2011, **511**, 336–339.
30 B. Wenger, M. Grätzel and J.-E. Moser, *J. Am. Chem. Soc.*, 2005, **127**, 12150–12151.
31 M. K. Nazeeruddin, R. Humphry-Baker, P. Liska and M. Grätzel, *J. Phys. Chem. B*, 2003, **107**, 8981–8987.